JOURNAL OF MAGNETIC RESONANCE, Series A 112, 112–117 (1995)

Linear Prediction with Singular-Value Decomposition for Removing Phase Artifacts in 2D VACSY Spectra

Y. K. LEE,* R. L. VOLD,† G. L. HOATSON,† Y.-Y. LIN, AND A. PINES‡

Materials Sciences Division, Lawrence Berkeley Laboratory, and Department of Chemistry, University of California, Berkeley, California 94720

Received June 6, 1994

Variable angle correlation spectroscopy (VACSY) has been successful as a two-dimensional NMR experiment for correlating isotropic and anisotropic interactions. The technique has been applied to studies of complex organic solids (*1*),[1] glasses (*2*), and molecular dynamics (*3*). However, one disadvantage of conventional 2D VACSY is that it is not possible to obtain pure-absorption-mode spectra because of "phase-twist" artifacts inherent to the experiment; the resulting loss of resolution and lineshape distortions may impede spectral analysis (*4*). In this Note, we describe the use of linear prediction with singular-value decomposition (LPSVD) to obtain absorption-mode 2D VACSY spectra free of artifacts.

Phase artifacts in an NMR spectrum can be viewed as truncation effects due to incomplete sampling of the time-domain Fourier space. First, consider a one-dimensional NMR signal:

$$S(t) = \int_{-\infty}^{\infty} I(\omega)\exp[i\omega t]d\omega. \qquad [1]$$

The spectral-intensity distribution, $I(\omega)$, may be obtained from Eq. [1] by a Fourier transformation. However, the final experimental spectrum, $I'(\omega)$, must take into account line broadening and truncation of the signal. Assuming that all spectral components have the same Lorentzian broadening, $I'(\omega)$ is obtained through a convolution of $I(\omega)$ with a Lorentzian point-spread function (PSF), $P(\omega)$:

$$I'(\omega) = I(\omega) * P(\omega). \qquad [2]$$

If the signal spans the full Fourier space for positive and negative time, $P(\omega)$ is an absorption Lorentzian lineshape, as shown in Fig. 1a. The function $I'(\omega)$ is then simply the broadened form of $I(\omega)$. If the signal spans only half of the Fourier space for positive time, $P(\omega)$ is complex valued (Fig. 1b),

$$P(\omega) = a(\omega) + id(\omega), \qquad [3]$$

where (*5*)

$$a(\omega) = \frac{\lambda}{\omega^2 + \lambda^2}$$

$$d(\omega) = \frac{\omega}{\omega^2 + \lambda^2}. \qquad [4]$$

Here, λ is the exponential damping factor and $a(\omega)$ and $d(\omega)$ are the absorption and dispersion Lorentzian lineshapes. In both cases the real part of $P(\omega)$ has the same lineshape and the same spectral information is available from spanning either all or just half of the time-domain Fourier space.

The same principle easily generalizes to higher dimensions. In two dimensions, the signal is written as

$$S(t_1, t_2) = \int_{-\infty}^{\infty} I(\omega_1, \omega_2)\exp[i(\omega_1 t_1 + \omega_2 t_2)]d\omega_1 d\omega_2. \qquad [5]$$

The experimental spectrum $I'(\omega_1, \omega_2)$ is a two-dimensional convolution of the spectral-intensity distribution, $I(\omega_1, \omega_2)$, with the 2D PSF, $P(\omega_1, \omega_2)$:

$$I'(\omega_1, \omega_2) = I(\omega_1, \omega_2) ** P(\omega_1, \omega_2). \qquad [6]$$

If there is no truncation and the signal spans the complete Fourier space, $P(\omega_1, \omega_2)$ is a 2D pure-absorption Lorentzian lineshape, as shown in Fig. 2a. If only half the Fourier space is acquired by truncating the signal for $t_2 < 0$, $P(\omega_1, \omega_2)$ is complex,

* Chemical Biodynamics Division, Lawrence Berkeley Laboratory, and Graduate Group in Biophysics, University of California, Berkeley, California 94720.

† Department of Physics, College of William and Mary, Williamsburg, Virginia 23187.

‡ To whom correspondence should be addressed at the University of California.

[1] Equations 10a and 10b in this reference should read: (10a) $\tan(\phi_{max}) = DW_i \cdot P_{2\,max}/DW_a$. (10b) $\tan(\phi_{min}) = DW_i \cdot P_{2\,min}/DW_a$.

1064-1858/95 $6.00

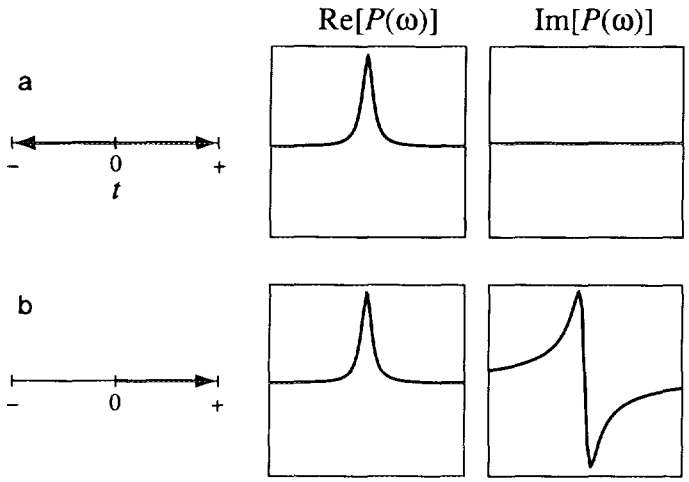

FIG. 1. One-dimensional Lorentzian point-spread function (PSF), $P(\omega)$. (a) Complete signal acquired for positive and negative time; $P(\omega)$ is then a real absorption Lorentzian lineshape. (b) Signal acquired only for $t > 0$. The real component is an absorption Lorentzian lineshape, while the imaginary component becomes a dispersion lineshape.

$$P(\omega_1, \omega_2) = 2a_1(\omega_1)[a_2(\omega_2) + id_2(\omega_2)]$$
$$= 2[a_1(\omega_1)a_2(\omega_2) + ia_1(\omega_1)d_2(\omega_2)], \quad [7]$$

where $a_1(\omega_1)$ is the absorptive component in ω_1, and $a_2(\omega_2)$ and $d_2(\omega_2)$ are absorptive and dispersive components in ω_2. Once again the pure-absorption lineshape, $a_1(\omega_1)a_2(\omega_2)$, can be obtained by sampling only half of the full Fourier space (Fig. 2b). Of course similar results may be obtained by truncating the signal along the t_1 dimension rather than t_2. If, however, both the t_1 and the t_2 dimensions are truncated, i.e., only one quadrant in the Fourier space is acquired, both the real and the imaginary components of $P(\omega_1, \omega_2)$ contain positive and negative lobes due to mixing of the absorptive and dispersive components (Fig. 2c),

$$P(\omega_1, \omega_2) = [a_1(\omega_1) + id_1(\omega_1)][a_2(\omega_2) + id_2(\omega_2)]$$
$$= [a_1(\omega_1)a_2(\omega_2) - d_1(\omega_1)d_2(\omega_2)]$$
$$+ i[a_1(\omega_1)d_2(\omega_2) + d_1(\omega_1)a_2(\omega_2)], \quad [8]$$

and pure-absorption lineshapes are no longer possible. Conventional methods of obtaining pure-absorption-mode 2D spectra include acquiring echoes in either the t_1 or the t_2 dimension (*6*) or acquiring both the +1 and the −1 coherence pathways in the t_1 dimension (*4, 7*). Both these methods ensure that the signal effectively spans two of the four quadrants in the 2D Fourier space.

In 2D VACSY, a series of variable angle spinning (VAS) free-induction decays are acquired and placed at angles (*8*)

$$\alpha = \tan^{-1}[RP_2(\cos\beta)] \quad [9]$$

in the signal-acquisition Fourier space defined by the "time" coordinates

$$t^a = P_2(\cos\beta)t$$
$$t^i = t, \quad [10]$$

as shown in Fig. 3. Here, t^a and t^i define the anisotropic and isotropic time axes, $P_2(\cos\beta)$ is the second Legendre polynomial, β is the angle of the rotation axis with respect to the static field, and R is the ratio of the anisotropic to isotropic spectral widths. Typically P_2 ranges from −0.5 to +0.5, so that the signal partially spans two of the quadrants in the Fourier space. Once the FIDs are positioned, the grid points within the shaded region, shown in Fig. 3, are interpolated from the experimental data points; the rest of the Fourier space is set to zero. The phase artifacts inherent to the 2D VACSY spectrum are due to incomplete sampling in these two quadrants.

Consider the PSF, $P(\omega^a, \omega^i)$, for $R = 2$ and $-0.5 \leq P_2 \leq +0.5$. Since α then ranges from −45° to +45°, the total area of the Fourier space spanned by the VACSY signal is equiv-

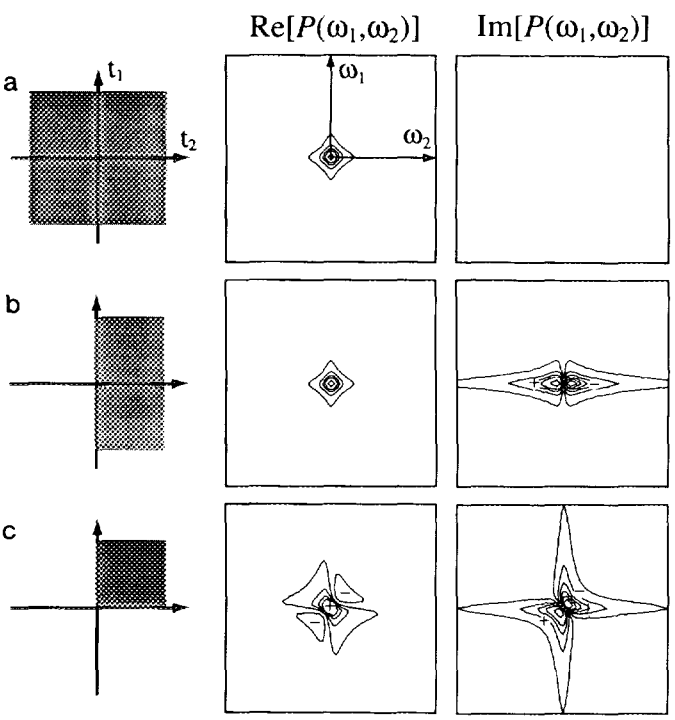

FIG. 2. Two-dimensional Lorentzian PSF, $P(\omega_1, \omega_2)$, in conventional 2D NMR experiments. (a) $P(\omega_1, \omega_2)$ for signal acquired in all four quadrants of the time-domain Fourier space. $P(\omega_1, \omega_2)$ is a real 2D Lorentzian lineshape. (b) $P(\omega_1, \omega_2)$ for signal acquired in two of the four quadrants. The real component of $P(\omega_1, \omega_2)$ remains a 2D absorption Lorentzian lineshape, $a_1(\omega_1)a_2(\omega_2)$, while the imaginary component is a mixture of absorptive and dispersive terms. (c) $P(\omega_1, \omega_2)$ for signal acquired in only one quadrant. $P(\omega_1, \omega_2)$ contains a mixture of absorptive and dispersive terms in both the real and the imaginary components.

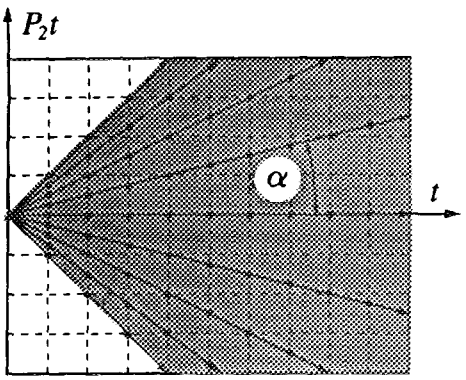

FIG. 3. Trajectories of variable angle spinning FIDs in the signal Fourier space defined by the variables $[P_2(\cos\beta)t, t]$. The dark lines represent the trajectory of the FIDs; the dots represent experimental data points, used to interpolate the points on the rectangular grid (dashed lines). The orientation of each FID is determined by the angle $\alpha = \tan^{-1}[RP_2(\cos\beta)]$.

alent to one quadrant. Thus $P(\omega^a, \omega^i)$, shown in Fig. 4a, is similar in form to $P(\omega_1, \omega_2)$ of Fig. 2c but rotated by 45°. The difference between the two PSFs is due to the star shape of the 2D Lorentzian (*5*). Had we used a cylindrically symmetric lineshape function, such as a 2D Gaussian, the two PSFs would differ only by the rotation. The artifact ridges become less intense when R increases and a larger area of the Fourier space contains data, as shown in Fig. 4b. Unfortunately this is achieved at the cost of spectral resolution in the anisotropic dimension and increased interpolation error. In addition, rearrangement of the FIDs will never completely remove the phase artifacts, since according to the Fourier projection slice theorem (*9*), the projection of the 2D VACSY spectrum onto the anisotropic ω^a axis is equal to the Fourier transformation of the slice along the t^a axis. The t^a axis, however, contains only one data point at $t^a = 0$, and its Fourier transformation is a constant function. Thus, as seen from Fig. 5a, the 2D VACSY spectrum must contain negative lobes to cancel out all spectral features in the projection. Similarly, the projection on to the isotropic ω^i axis will result in a pure-absorption MAS spectrum despite the phase artifacts.

The spectral artifacts in Fig. 5 are unique to 2D VACSY experiments due to the unconventional truncation and interpolation of the time-domain data. Since the FIDs are placed symmetrically about the t^i axis, the slice of the VACSY PSF along the ω^a axis contains no dispersive terms, while the width of the lineshape varies depending on the level of truncation determined by R (Fig. 4). Thus even using a magnitude calculation, each anisotropic pattern appears absorptive provided there is no significant interference of the phase artifacts from the different isotropic sites in the spectrum. Often these artifacts may be ignored, particularly when the spectrum is dominated by broad anisotropic patterns, since then the artifacts also broaden, and the interference between different sites becomes negligible. This explains the success of 2D VACSY despite the artifacts inherent to the technique. However, these artifacts can become a serious problem when the spectrum contains closely spaced isotropic shifts with small anisotropies. The ridge artifacts emerging from a narrow site may interfere with the anisotropic patterns of neighboring sites, causing lineshape distortions. The removal of such artifacts becomes especially important when there are partially overlapping or a continuous distribution of isotropic shifts, or when accurate lineshape analysis is required, as in the study of intermediate dynamics or partial molecular ordering.

Artifacts in 2D VACSY spectra can be reduced if the missing points in the signal Fourier space can be extrapolated using the experimental data. However, due to the large number of missing data points, the extrapolation technique must maintain accuracy over several cycles of the signal. Linear prediction with singular-value decomposition is one such technique that has been used for extrapolation and spectral estimation in NMR to improve resolution and signal-to-noise ratios (*10, 11*). It has also been used to minimize artifacts in pulsed ESR spectra

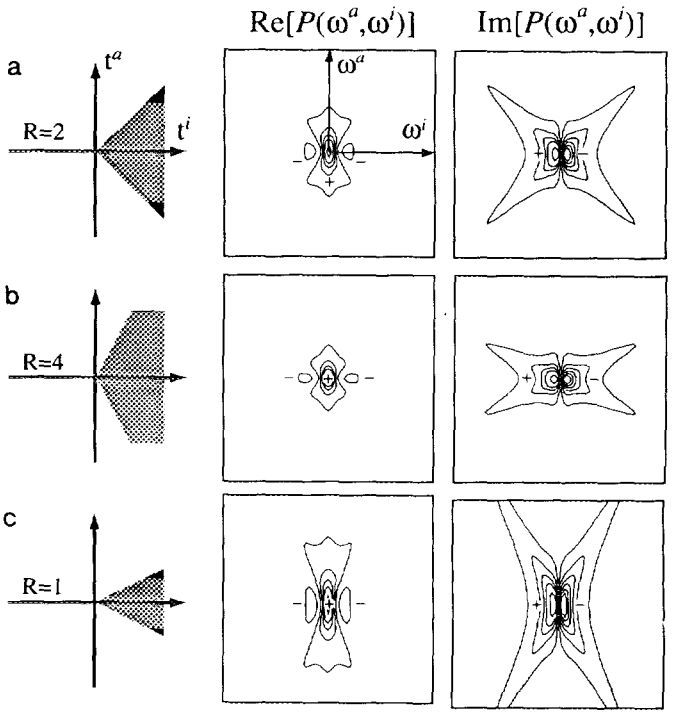

FIG. 4. Two-dimensional Lorentzian PSF, $P(\omega^i, \omega^a)$, for 2D VACSY experiments. All functions are calculated using $-0.5 \leq P_2 \leq +0.5$. The different values for R determine the overall area of the time-domain Fourier space covered by the data, as shown by the shaded regions. (a) $P(\omega^i, \omega^a)$ with $R = 2$. The total area containing data is equivalent to one quadrant. $P(\omega^i, \omega^a)$ is similar in form to $P(\omega_1, \omega_2)$ in Fig. 2c but rotated by 45°. (b) $P(\omega^i, \omega^a)$ with $R = 4$. The intensity of the ridge artifacts decreases as a larger area of the time-domain Fourier space is filled with data, and the overall width of $P(\omega^i, \omega^a)$ at $\omega^i = 0$ is narrower than that in (a). (c) $P(\omega^i, \omega^a)$ with $R = 1$. The ridge artifacts are more intense and lineshapes are broader at $\omega^i = 0$.

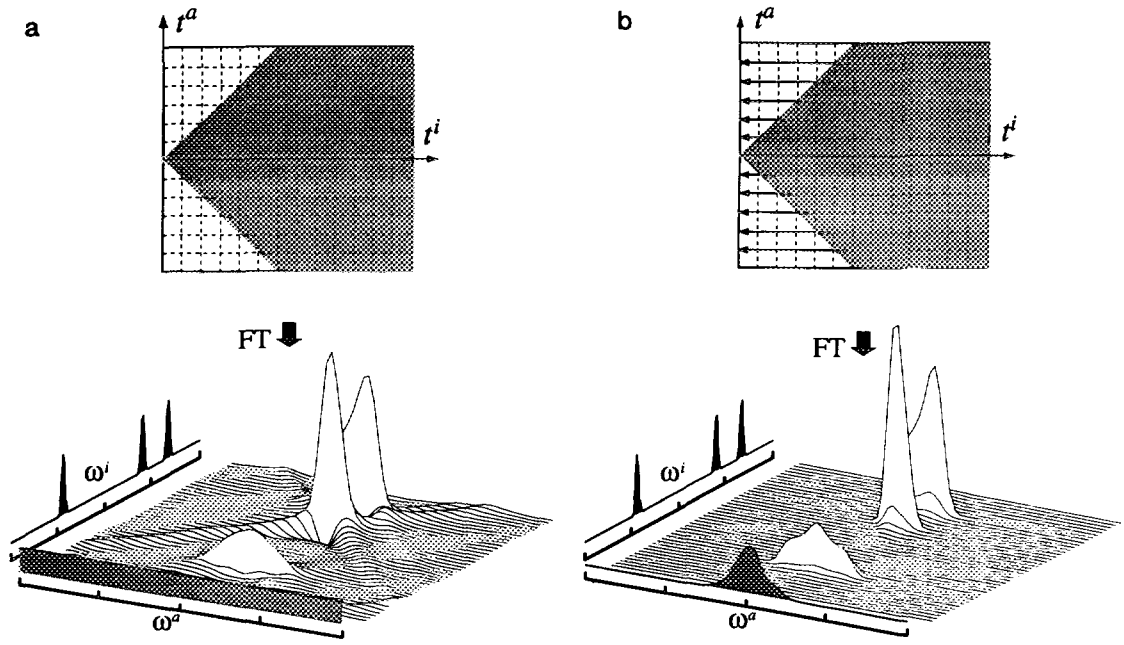

FIG. 5. Simulation of 2D VACSY spectra. The simulations were made using $R = 2$, $t_d = 200$ μs, and three sites with the chemical-shift tensors: (σ_{xx}, σ_{yy}, σ_{zz}) = (0.3, 1.0, 2.3), (−0.5, −0.5, −1.5), (−2.5, −2.0, −1.0) (kHz). (a) Normal phased 2D VACSY spectrum obtained using $-0.5 \leq P_2 \leq +0.5$ and $R = 2$. The area of the Fourier space outside of the shaded region is set to zero. The 2D spectrum reveals the phase artifacts inherent to the normal 2D VACSY experiment. The projection onto the ω^a axis yields a constant function, whereas the projection onto the ω^i axis yields the pure absorption isotropic spectrum. (b) 2D VACSY spectrum after extrapolation using LPSVD. The area set to zero in (a) is extrapolated from the interpolated simulation data in the shaded region. LPSVD is used to extrapolate the data in each slice, parallel to the t^a axis, to the $t^i = 0$ point. The phase artifacts are eliminated from the 2D spectrum. The projection onto the ω^a axis yields the overlap of the different traceless anisotropic powder patterns, while the projection onto the ω^i axis again yields the isotropic MAS spectrum.

(*12*). The LPSVD method assumes the signal to be a time series represented by a sum of decaying exponentials with the addition of white Gaussian noise, $w(n)$ (*13*),

$$y_n = \sum_{m=1}^{M} a_m \exp[(i\omega_m - \lambda_m)t_d(n + \delta)] + w(n),$$
$$n = 0, 1, \ldots, N-1, \qquad [11]$$

where a_m, ω_m, λ_m are the complex amplitude, frequency, and damping factor of each exponential term, respectively, M is the total number of exponential components, t_d is the dwell time of the time-series signal, N is the total number of points in the time series, and δ is an integer that specifies the shift from the time origin to the first sampled data point.

We now briefly discuss the steps involved in the LPSVD computation; more complete presentations may be found elsewhere (*10, 11, 13, 14*). A set of linear prediction (LP) equations may be set up in backward mode as

$$\begin{bmatrix} y_1 & y_2 & \cdots & y_L \\ y_2 & y_3 & \cdots & y_{L+1} \\ \vdots & \vdots & \ddots & \vdots \\ y_{N-L} & y_{N-L+1} & \cdots & y_{N+1} \end{bmatrix} \begin{bmatrix} b_0 \\ b_1 \\ \vdots \\ b_{L-1} \end{bmatrix} = - \begin{bmatrix} y_0 \\ y_1 \\ \vdots \\ y_{N-L-1} \end{bmatrix}, \qquad [12]$$

or in brief form as

$$\mathbf{Ab} = -\mathbf{h}, \qquad [13]$$

where **b** is the vector of the backward LP coefficients, **A** is the $(N-L) \times L$ data matrix, and **h** is the data vector with $N-L$ components. The number of LP coefficients (prediction order), L, is bounded by the condition $M \leq L \leq N - M$, but is typically set to $0.75N$ (*13*).

The singular-value decomposition (SVD) of the matrix **A** may be written as a product of three matrices (*14*),

$$\mathbf{A} = \mathbf{U}\begin{bmatrix} \mathbf{S} \\ \mathbf{O} \end{bmatrix}\mathbf{V}^{\dagger}, \qquad [14]$$

where † denotes Hermitian conjugate; **U** and **V** are orthogonal matrices of dimensions $(N-L) \times (N-L)$ and $L \times L$, respectively; **S** is a diagonal matrix with the singular values $\{\sigma_k, k = 1, 2 \cdots \min(L, N-L)\}$ as its diagonal elements; and **O** is a null matrix. Denoting the column vectors of the matrices **U** and **V** by $\{\mathbf{u}_1, \mathbf{u}_2, \ldots, \mathbf{u}_{N-L}\}$ and $\{\mathbf{v}_1, \mathbf{v}_2, \ldots, \mathbf{v}_L\}$, the backward linear prediction coefficients are computed as

$$\mathbf{b} = -\sum_{m=1}^{M} \frac{1}{\sigma_m}(\mathbf{u}_m^{\dagger}\mathbf{h})\mathbf{v}_m, \quad [15]$$

where the summation limit, M, truncates the SVD solution for $\mathbf{b}$. For low-noise data, M is simply the total number of peaks in the spectrum; if, however, the data contain significant noise, M becomes an adjustable parameter that may be chosen to have a higher value (*15, 16*). Once the backward LP coefficients have been calculated, the missing data points in the time series in Eq. [11] may be extrapolated as

$$y_n = -\sum_{k=1}^{L} b_k y_{n+k}, \quad n = (-1, -2, \ldots, -\delta), \quad [16]$$

where $n = -\delta$ specifies the data point at the time origin. However, to take advantage of the signal-to-noise ratio improvements in LPSVD, the entire time series should be reconstructed by calculating the spectral parameters associated with the data set. The parameters, α_m and ω_m, can be obtained by constructing a polynomial

$$B(z) = 1 + b_1^* z^{-1} + b_2^* z^{-2} + \cdots + b_L^* z^{-L}, \quad [17]$$

which has roots at $z_m = \exp[i\omega_m + \alpha_m]$. The complex amplitude, a_m, can then be obtained by substituting α_m and ω_m back into Eq. [12].

The 2D VACSY signal after interpolation may be written in the same discrete time-series form as Eq. [11],

$$y_{n^a,n^i} = \sum_{m=1}^{M} a_{m,n^a} \exp[i\omega_m^i t_d n^i - \lambda_m], \quad [18]$$

where

$$a_{m,n^a} = \int I(\omega_m^i, \omega^a)\exp[i\omega^a t_d n^a/R]d\omega^a. \quad [19]$$

Here, $I(\omega_m^i, \omega^a)$ is the 2D correlated isotropic–anisotropic spectrum, while n^i and n^a specify the discrete time increments in the t^i and t^a dimensions. Since the VACSY spectrum correlates isotropic frequencies with distributions of anisotropic frequencies, only the sequence of data points parallel to the t^i axis can be assumed to form a time series represented by a sum of decaying exponentials. Thus LPSVD must be applied to each slice parallel to the t^i axis to extrapolate the missing data and completely fill two of the quadrants in the time-domain Fourier space, as shown in Fig. 5b.

The advantages of using LPSVD with experimental 2D VACSY data are demonstrated by ^{13}C NMR of solid lauric acid. All spectra were recorded at 7.07 T with a ^{13}C resonant frequency of 75.40 MHz. Lauric acid poses a particularly difficult problem for the VACSY technique because of the combination of a large spectral width and small chemical-shift anisotropies of the aliphatic sites. Four isotropic resonances are completely resolved in the MAS spectrum, which contains the carboxyl resonance at 181 ppm and three aliphatic resonances centered about 24 ppm. Thirty-one VAS FIDs were acquired, each containing 512 points and using angles restricted to the range $-0.5 \leq P_2(\cos\beta) \leq 0.5$. After interpolation onto a 128 × 512 grid, LPSVD computations were carried out with MATLAB-SGI (Version 4.0), using matrix software developed by the LINPACK (*17*) and EISPACK (*18*) projects. The signal parameters for each n^a slice parallel to the t^i axis were obtained using $N = 512 + n_a - 65$ for $n_a \leq 65$ and $N = 512 - n_a + 65$ for $n_a > 65$ and $L = 284$. The profile of the M values used in the computations, shown in Fig. 6, was determined empirically by comparing Fourier transformations of several n^a slices with and without LPSVD. This ensures that for each n^a slice the signal parameters obtained from LPSVD reproduced the correct experimental spectrum.

Figure 7 shows the MAS spectrum and the anisotropic patterns obtained from a 2D VACSY experiment. The assignments for the different isotropic ^{13}C sites are based on liquid-state ^{13}C NMR spectra (*19*). The spectra in column I were obtained directly through Fourier transformation, while the spectra in column II were obtained using the LPSVD spectral estimation method described above. Fourier transformation directly after interpolation results in severe artifact interference among the aliphatic carbon resonances b, c, and d, making examination of individual anisotropic patterns difficult. The ridge artifacts from site b can even be seen in the anisotropic spectrum of the carboxyl carbon (site a), appearing as lobes on both sides of the powder pattern. These spectral artifacts are significantly reduced using LPSVD as shown in column II. In particular, site a shows that the anisotropic lineshape remains unchanged when LPSVD is used, while the artifact lobes are completely removed. Comparable results (not shown) have also been obtained using the commercial LPSVD routine in FELIX data-

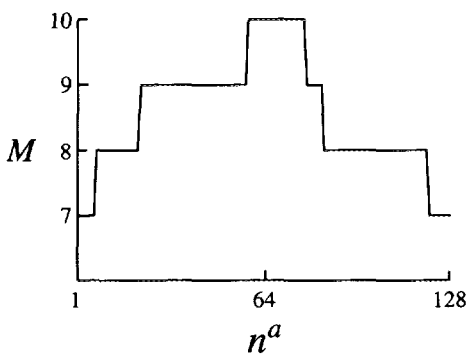

FIG. 6. Profile of the M parameter used for LPSVD processing, as described in the text. The M value used for extrapolation varied, depending on the anisotropic slice index, n^a.

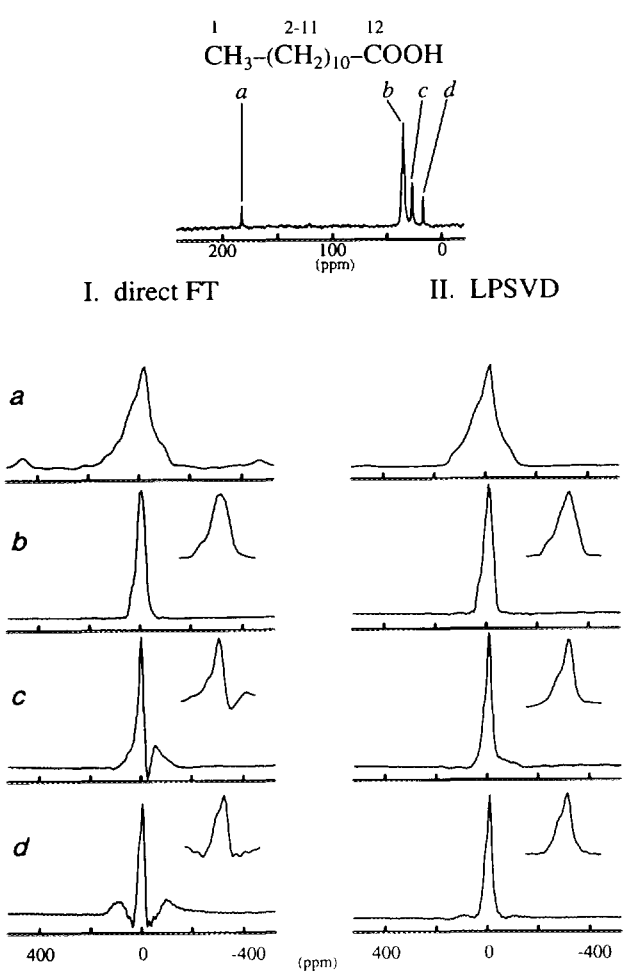

FIG. 7. The isotropic and anisotropic spectra obtained from a 2D VACSY spectrum of lauric acid. The MAS spectrum, in ppm units relative to TMS, reveals four completely resolved sites. Site a corresponds to the carboxyl carbon 1, site b to carbons 4–10 and 2; site c to carbons 3 and 11, and site d to the methyl carbon 12. The anisotropic patterns in column I were obtained by Fourier transforming the interpolated data with zeros outside of the region spanned by the FIDs. The anisotropic patterns in column II were obtained using LPSVD to construct a data set that completely spanned two of the four quadrants in the time-domain Fourier space.

processing software (Biosym Technologies). Further analysis and interpretation of the anisotropic lineshapes of lauric acid and lauric acid in an inclusion compound will be presented elsewhere.

In summary, we have shown that 2D VACSY artifacts have the same origin as the phase-twist artifacts observed in conventional 2D NMR experiments. These artifacts may be removed by using LPSVD to fill in missing data in the time-domain Fourier space. The resulting pure-absorption spectrum eliminates resolution problems associated with closely spaced isotropic lines and interference of phase artifacts. This should allow 2D VACSY to be applied to investigate a wider range of complex systems. Similar spectral-analysis methods may be applicable to the 3D VACSY exchange experiments that also suffer from artifacts due to holes in the time-domain Fourier space (*20*).

ACKNOWLEDGMENTS

This work was supported by the Director, Office of Energy Research, Office of Basic Energy Sciences, Material Sciences Division, and Office of Health and Environmental Research, Health Effects Research Division, of the U.S. Department of Energy under Contract DE-AC03-76SF000098 and National Science Foundation Grant CHE-930557. G.L.H. and R.L.V. thank Alex Pines and his research group for their hospitality.

REFERENCES

1. L. Frydman, G. C. Chingas, Y. K. Lee, P. J. Grandinetti, M. A. Eastman, G. A. Barrall, and A. Pines, *J. Chem. Phys.* **97,** 4800 (1992).
2. J. W. Zwanziger, K. K. Olsen, and S. L. Tagg, *Phys. Rev. B* **47,** 14,618 (1993).
3. L. Frydman, S. Vallabhaneni, Y. K. Lee, and L. Emsley, *J. Chem. Phys.* **101,** 111 (1994).
4. D. J. States, R. A. Haberkorn, and D. J. Ruben, *J. Magn. Reson.* **48,** 286 (1982).
5. R. R. Ernst, G. Bodenhausen, and A. Wokaun, "Principles of Nuclear Magnetic Resonance in One and Two Dimensions," Clarendon Press, Oxford, 1987.
6. A. Bax, A. F. Mehlkopf, and J. Smidt, *J. Magn. Reson.* **35,** 373 (1979).
7. J. Keeler and D. Neuhaus, *J. Magn. Reson.* **63,** 454 (1985).
8. L. Frydman, Y. K. Lee, L. Emsley, G. C. Chingas, and A. Pines, *J. Am. Chem. Soc.* **115,** 4825 (1993).
9. K. Nagayama, P. Bachmann, K. Wüthrich, and R. R. Ernst, *J. Magn. Reson.* **31,** 133 (1978).
10. H. Barkhuijsen, R. De Beer, W. M. M. J. Bovee, and D. Van Ormondt, *J. Magn. Reson.* **61,** 465 (1985).
11. D. S. Stephenson, *Prog. NMR Spectrosc.* **20,** 515 (1988).
12. J. Gorcester and J. H. Freed, *J. Magn. Reson.* **78,** 292 (1988).
13. R. Kumaresan, and D. W. Tufts, *IEEE Trans. Acoust. Speech Signal Process.* **ASSP-30,** 833 (1982).
14. S. M. Kay, "Modern Spectral Estimation Theory and Application," Prentice-Hall, Englewood Cliffs, New Jersey, 1988.
15. R. De Beer, D. Van Ormondt, W. W. F. Pijnappel, and J. W. C. Van Der Veen, *Isr. J. Chem.* **28,** 249 (1988).
16. Y.-Y. Lin, N.-H. Ge, and L.-P. Hwang, *J. Magn. Reson. A* **105,** 65 (1993).
17. J. J. Dongarra, C. B. Moler, J. R. Bunch, and G. W. Steward, "LINPACK User's Guide," SIAM, Philadelphia, 1979.
18. B. T. Smith, J. M. Boyle, J. J. Dongarra, B. S. Garbow, Y. Ikebe, V. C. Klema, and C. B. Moler, "Matrix Eigensystem Routines—EISPACK Guide, Lecture Notes in Computer Science," Springer-Verlag, Berlin, 1977.
19. E. Bengsch, B. Perly, C. Deleuze, and A. Valero, *J. Magn. Reson.* **68,** 1 (1986).
20. Y. K. Lee, L. Emsley, R. G. Larsen, K. Schmidt-Rohr, M. Hong, L. Frydman, G. C. Chingas, and A. Pines, *J. Chem. Phys.* **101,** 1 (1994).